Journal of Solid State Chemistry 183 (2010) 1215–1220

Contents lists available at ScienceDirect

Journal of Solid State Chemistry

journal homepage: www.elsevier.com/locate/jssc

$Ca_4Fe_{3-x}Mn_xO_{8-\delta}Cl_2$: A new $n=3$ Ruddlesden–Popper oxychloride

Tao Yang [a], Junliang Sun [b], Mark Croft [c], Israel Nowik [d], Alexander Ignatov [e], Rihong Cong [f], Martha Greenblatt [a,*]

[a] Department of Chemistry and Chemical Biology, Rutgers, The State University of New Jersey, 610 Taylor Road, Piscataway, NJ 08854-8087, USA
[b] Structural Chemistry, Stockholm University, SE-10691 Stockholm, Sweden
[c] Department of Physics and Astronomy, Rutgers, The State University of New Jersey, 136 Frelinghuysen Road, Piscataway, NJ 08854, USA
[d] Racah Institute of Physics, The Hebrew University, Jerusalem 91904, Israel
[e] Materials Science and Engineering Department, Rutgers University, Piscataway, NJ 08854, USA
[f] College of Chemistry and Molecular Engineering, Peking University, Beijing 100871, PR China

ARTICLE INFO

Article history:
Received 5 February 2010
Received in revised form
10 March 2010
Accepted 11 March 2010
Available online 18 March 2010

Keywords:
Ruddlesden–Popper
Oxychloride
Iron
Manganese
Structure

ABSTRACT

Solid state solutions of $Ca_4Fe_{3-x}Mn_xO_{8-\delta}Cl_2$ ($0.92 \le x \le 1.79$ ($\delta \sim 0.1$) single crystals were synthesized in $CaCl_2$-flux in air. The structure, determined by single-crystal X-ray diffraction, is related to the $n=3$ Ruddlesden–Popper phase in space group $I4/mmm$ with strong deviations from the ideal structure. Mn and Fe are disordered over two transition metal sites. Due to the positional disordering of the equatorial oxygen atoms in the MO_6 octahedra in $Ca_4Fe_{3-x}Mn_xO_{8-\delta}Cl_2$ both tilting ($\sim 9^\circ$) along the c-axis and rotation ($\sim 10.5^\circ$) within the ab-plane are observed. All the Fe ions are trivalent, as confirmed by ^{57}Fe Mössbauer spectroscopy and X-ray absorption near edge spectroscopy (XAS), while the formal valence state of Mn varies from very close to 4+ in the $x=0.92$ to mix-valent 3+/4+ in the $x=1.79$ member, as indicated by XAS. Magnetic investigations evidence short-range antiferromagnetic ordering already at room temperature and spin-glass behavior at low temperature due to the structural disordering of Mn/Fe.

1. Introduction

Manganese-contained perovskites and Ruddlesden–Popper (RP) phases have been the subject of intense research, primarily because of their complex magnetic, electric transport and colossal magnetoresistance (CMR) properties [1,2]. The Mn-RP phases, with the general formula $(AO)(AMnO_3)_n$ (A=rare earth or alkali earth metal; $n=1, 2, 3, \ldots, \infty$), have structures consisting of alternate stacking of $nAMnO_3$ perovskite block layers separated by an AO rock-salt-type layer. In RP manganites the Mn–O–Mn interactions are interrupted by the nonmagnetic AO layers, and thus display two-dimensional (2D) properties. It is well known that electron correlations are enhanced in 2D materials. Up to now, Ca_2MnO_4, $Ca_3Mn_2O_7$, $Ca_4Mn_3O_{10}$, Sr_2MnO_4, $Sr_3Mn_2O_7$ with the RP structure have been reported, all with Mn in formal valence state 4+ [3–8]. It is generally agreed that the nonintegral oxidation state of Mn ($Mn^{3+/4+}$) is the main cause of CMR. Thus, electron-doped RP manganites, including substitutions by rare earth for the alkaline earth A site or high valent transition metal ions (e.g., V^{5+}, Nb^{5+}, Mo^{6+}, etc.) for Mn, to realize mixed-valent Mn, are extensively studied [9–12]. A notable example was the observation of a large CMR of ~20,000% in a single-crystal of $La_{1.2}Sr_{1.8}Mn_2O_7$ [2]. The substitution of oxygen by halide ions can also reduce the metal oxidation state in RP manganites. Up to now, two manganese-containing oxyhalides have been prepared: Sr_2MnO_3Cl, $Sr_4Mn_3O_{7.56}Cl_2$ [13,14], with the formal valence states ~3+. In addition to manganites, only a few transition metal RP oxyhalides in a single valence state (Cu^{2+}, Co^{2+}, Co^{3+} or Fe^{3+}) are reported [15–23]. We successfully synthesized by the flux method, a new series of RP-Mn-oxychloride single crystals: $Ca_4Fe_{3-x}Mn_xO_{8-\delta}Cl_2$ ($0.92 \le x \le 1.79$). Mn and Fe are extensively disordered over two independent crystal sites. According to ^{57}Fe Mössbauer and X-ray absorption near edge spectroscopies (XAS), all the Fe ions are trivalent, while the formal valence state of Mn varies from very close to 4+ in the $x=0.92$ member mix-valent 3+/4+ in the $x=1.79$ member.

2. Experiment section

$Ca_4Fe_{3-x}Mn_xO_{8-\delta}Cl_2$ ($0.92 \le x \le 1.79$) were prepared in an open system, with $CaCl_2$ as flux at 850 °C. In a typical synthesis, a powder precursor was prepared by heating $CaCO_3$ (Aldrich, 99.995%), Mn_2O_3 (Aldrich, 99.999%) and Fe_2O_3 (Aldrich, 99.98%) in a ratio of $4{:}x{:}3-x$ ($0 \le x \le 3$; 0.1–0.2 g of the precursor and

* Corresponding author. Fax: +1 732 445 5312.
E-mail addresses: martha@rutchem.rutgers.edu, greenblatt@rutchem.rutgers.edu (M. Greenblatt).

0022-4596/$ - see front matter © 2010 Elsevier Inc. All rights reserved.
doi:10.1016/j.jssc.2010.03.019

2–3 g $CaCl_2$–$2H_2O$ (Aldrich, >99.0%) was placed in a 5 mL Al_2O_3 crucible. The mixture was then slowly heated to 850 °C and kept for 30–40 h, and then the furnace was shut off and allowed to cool to room temperature in a few hours. The small amount of $CaCl_2$, that remained in the crucible after the reaction, was washed away with water to yield $Ca_4Fe_{3-x}Mn_xO_{8-\delta}Cl_2$ shiny plate-like black single crystals.

The title compounds were obtained unintentionally, because our original objective was to synthesize A site ordered perovskite "$CaMn_3Fe_4O_{12}$" by the flux method. Initially the Mn:Fe ratios in the starting materials were 1:6, 2:5, 3:4, 4:3, 5:2, 6:1. We were able to obtain single-phase products, only with Mn:Fe ratios between 2:5 and 4:3. The purities of all the single-phase products were checked by powder X-ray diffraction (PXD), and the ratio of Mn:Fe were analyzed by ICP. Fig. 1a is representative of the Le Bail refinement result in space group *I*4/*mmm* with Topas [24]. Fig. 1b shows the PXD patterns of six pure samples and the inset shows the variation of the cell parameters with *x*. The PXD pattern of the sample with $x=0.92$ contains a small unindexed peak at ~10.4° from an impurity (<1%); although the plot of lattice parameters vs. composition suggests that the true *x* of this "$x=0.92$" is really $x=1.0$–1.1 (Fig. 1b, inset), subsequent discussion of this sample will refer to the ICP results of $x=0.92$. Single-crystal X-ray diffraction data of the sample with $x=1.36$ were collected at room temperature on an Xcalibur3 diffractometer equipped with a CCD camera and Mo*K*α radiation ($\lambda=0.71073$ Å). The structure solution and refinement were carried out with the SHELX-97 software package [25]. Crystal parameters, atomic coordinates and selected bond-distances are listed in Tables 1–3. PXD data were recorded on a Bruker D8-Advance diffractometer (in Bragg–Brentano geometry with Cu*K*α radiation $\lambda=1.5418$ Å, SOL-X solid state detector, 40 kV and 30 mA). ^{57}Fe Mössbauer spectroscopy studies were performed with a conventional constant acceleration drive and a 100 mCi ^{57}Co:Rh source. The velocity calibration was made with a room temperature α-Fe absorber, and the isomer shift (I.S.) values reported are relative to that of the iron absorber. XAS measurements were collected simultaneously in both the transmission and fluorescence modes

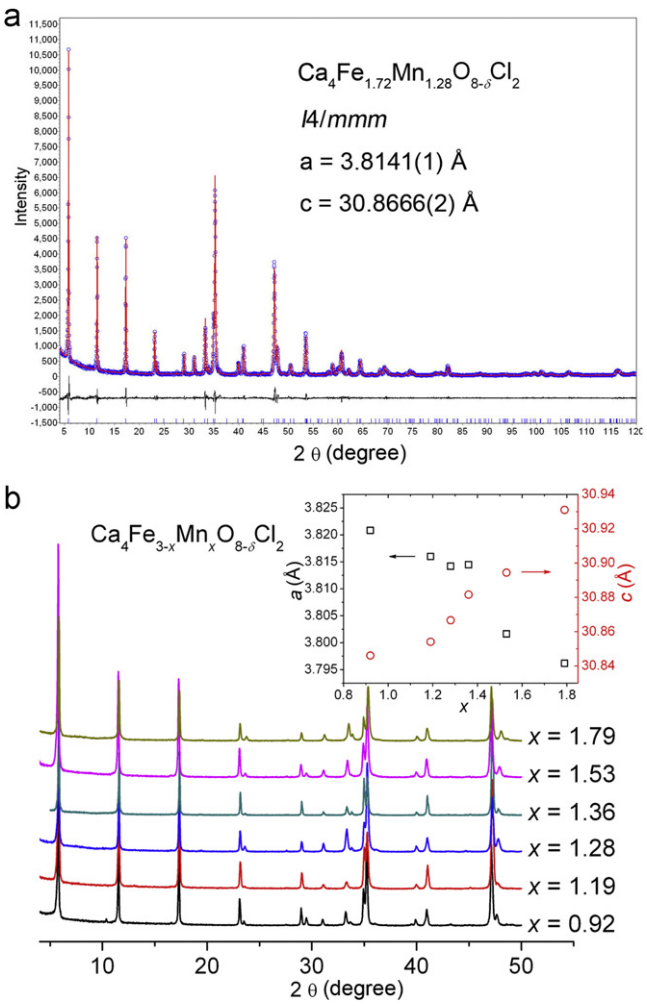

Fig. 1. (a) Example of Le Bail refinement for $x=1.28$ sample and (b) PXD patterns with *x* in the range between 0.92 and 1.79. The inset shows the variation of the cell parameters with *x* as obtained from the Le Bail refinements.

Table 1
Crystallographic parameters of $Ca_4Mn_{1.36}Fe_{1.64}O_8Cl_2$.

Formula	$Ca_4Mn_{1.36}Fe_{1.64}O_8Cl_2$
Formula mass	525.13
Radiation λ (Å)	0.71073
Crystal size (mm)	$0.01\times0.07\times0.08$
Morphology	Plate-like, black
Space group	Tetragonal, *I*4/*mmm*
a (Å)	3.7960(5)
c (Å)	30.846(6)
V (Å^3)	444.48(12)
Z	2
ρ_{calcd} (g/cm^3)	3.924
μ (Mo*K*α) (mm^{-1})	7.398
Reflections collected	8035
Independent reflections	372
$I>2\sigma(I)$	304
R_{int}	0.0355
θ range (degree)	3.96–35.72
GOF	0.986
R_1/wR_2^a ($I>2\sigma(I)$)	0.0364/0.0928
R_1/wR_2 (all data)	0.0466/0.0968

Table 2
Atomic coordinates of $Ca_4Mn_{1.36}Fe_{1.64}O_8Cl_2$ from the X-ray diffraction refinement.

Atom	Position	*x*	*y*	*z*	U_{eq}/Å^2	Occup.
Mn1	2b	0.5	0.5	0	0.0071(3)	0.57
Fe1						0.43
Mn2	4e	0.5	0.5	0.87856(3)	0.0095(2)	0.57
Fe2						0.43
Ca1	4e	0	0	0.94094(7)	0.0269(4)	1
Ca2	4e	0	0	0.17920(5)	0.0155(3)	1
Cl	4e	0.5	0.5	0.21653(6)	0.0250(4)	1
O1A	8g	0.5	0	0.0114(7)	0.024(7)	0.21(4)
O1B	8i	0.593(3)	0	0	0.019(5)	0.29(4)
O2	16n	0.078(5)	0	0.4390(2)	0.024(5)	0.25
O3	8g	0.5	0	0.13097(15)	0.0264(9)	1

Table 3
Selected bond distances (Å) in $Ca_4Mn_{1.36}Fe_{1.64}O_8Cl_2$ from the X-ray diffraction refinement.

Bond	Length	Bond	Length
Ca1–O1A/O1B(×4)	2.400(9)/2.895(10)	Mn1/Fe1–O1A/O1B(×4)	1.930(2)
Ca1–O2(×4)	2.485(12)/2.901(13)	Mn1/Fe1–O2(×2)	1.904(8)
Ca1–O3(×4)	2.920(4)		
Ca2–O3(×4)	2.412(3)	Mn2/Fe2–O2	1.888(8)
Ca2–Cl(×4)	2.9207(10)	Mn2/Fe2–O3(×4)	1.9207(8)
Ca2–Cl	3.216(2)	Mn2/Fe2–Cl	2.9331(9)

on powder samples on beam line X-19A at the Brookhaven National Synchrotron Light Source. The magnetic measurements were carried out on powder samples with a Quantum Design MPMS-XL superconducting quantum interference device (SQUID) magnetometer.

3. Results and discussion

Only two $n=3$ oxyhalides have been reported so far: $Sr_4Mn_3O_{7.56}Cl_2$ [13,14] and $Sr_4Co_3O_{7.5}Cl_2$ [15]. Their oxygen contents were determined from Rietveld refinements of powder neutron diffraction data. Different from our experiments, both of the above compounds were prepared in an evacuated quartz tube, which might account for Mn and Co being mostly trivalent, while the phases reported here, $Ca_4Fe_{3-x}Mn_xO_{8-\delta}Cl_2$ were prepared in air, with formally Fe^{3+} and Mn^{4+} ions.

Fig. 2a is the ideal representation of the $n=3$ RP-Mn-oxychloride. The structure contains two unique polyhedra of Mn/Fe, which are statistically disordered throughout the structure (discussed later). M1 (Mn1/Fe1) is coordinated by 6O in a typical octahedral environment with the metal–oxygen distance in the range of 1.904(8) and 1.930(2) Å. M2 (Mn2/Fe2) is considered to be in a square pyramidal coordination environment with 5O at distances 1.888(8) and 1.9207(8) Å) and 1Cl at a distance of 2.9331(9) Å); M2 is strongly displaced from the plane of O3 towards O2, and the O3–M2–O3 angle is ~162.3°, comparable

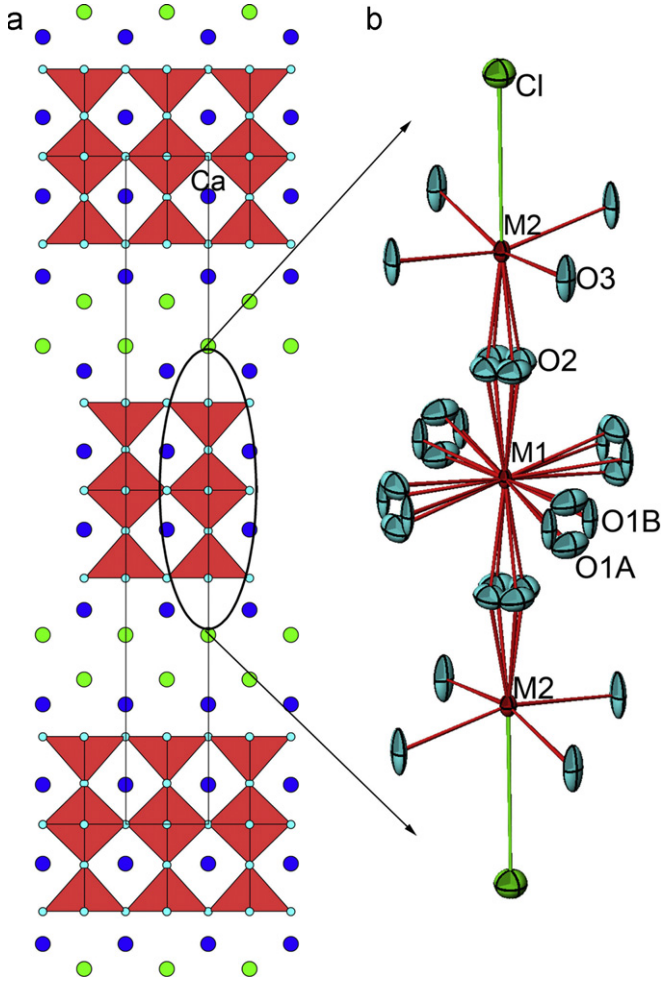

Fig. 2. (a) Average structural view along the [1 0 0] direction and (b) enlargement of the transition metal coordination, where O1 and O2 are split into partially occupied atoms around the special position.

with those in its analogs $Sr_4Mn_3O_{7.56}Cl_2$ (~165.6°) [13,14] and $Sr_4Co_3O_{7.5}Cl_2$ (~164.4°) [15]. When the simplest structure model (Fig. 2a) was applied for refining the single-crystal diffraction data, the two oxygen atoms (O1 and O2), initially placed in special positions 4*c* and 4*e*, respectively, showed unusually large anisotropic thermal parameters (plate-like ellipsoid of the displacement parameters), a clear indication of structural splitting and even possible partial occupancy. The analogs of the title compounds, $Sr_4Mn_3O_{7.56}Cl_2$ [13,14] and $Sr_4Co_3O_{7.5}Cl_2$ [15], were reported to possess about 1/4 deficiency in the in-plane oxygen position (O1 in our structure) determined by powder neutron diffraction (PND). In both of these analogs, O1 is slightly shifted along the *a* direction to a lower symmetry position.

In our compound, there seems to be no vacancy at the O2 site. Since the M2–Cl bond is long, if there were any O2 deficiency, M2 would be mainly coordinated by 4 oxygen atoms in a close-to-planar environment, which is unlikely. Thus, the large anisotropic displacement parameter of O2 is strong indication of structural splitting. Therefore O2 was placed in a lower symmetry position (16*n*) with a 0.25 occupancy factor in the final refinement.

The O1 case is somewhat more complex. According to its plate-like anisotropic thermal parameters, O1 was split into four positions (two unique positions, O1A (8g) and O1B (8i)), and the refinement improved in this way with reasonable Mn1–O1 distances. From the final thermal ellipsoids of O1A and O1B, it is seen that O1 may form a circle around the original O1 position instead of just four positions of the present treatment (Fig. 2b). O1 may also be deficient like the analogs discussed above. Thus two structural models, with (O1A+O1B) either 100% or 75% occupancy (it will be explained later why 1/4 deficiency was chosen), were refined. The 100% case refined to a R_1 factor of 0.0466, while the 75% one to a R_1 factor of 0.0549. Evidently from the X-ray diffraction data, an unambiguous determination of O1 deficiency in $Ca_4Fe_{3-x}Mn_xO_{8-\delta}Cl_2$ is not possible.

We note that the structure of $Ca_4Mn_3O_{10}$ RP phase also deviates considerably from the ideal RP model (*I*4/*mmm*). The MnO_6 octahedra tilt (~12°) along the *c*-axis and a rotate (~10°) in the *ab*-plane, which result in an enlarged unit cell in the orthorhombic space group *Pbca* (see Fig. S1 in the Supporting Information) [26]. The tilting of the MnO_6 octahedra in the $a^-a^-c^+$ model of $Ca_4Mn_3O_{10}$ is a consequence of the small unit cell dimension within the perovskites layer ($a_p=a/\sqrt{2}\sim3.72$ Å). With $A=Sr^{2+}$, there are only two known $n=3$ RP oxychlorides: $Sr_4Mn_3O_{7.56}Cl_2$ [13,14] and $Sr_4Co_3O_{7.5}Cl_2$ [15], whose structures were refined based on PND data. Both compounds show ~1/4 vacancy of O1, but no tilting of the octahedra, probably due to the relatively large *a* parameters: 3.9012(2) Å for $Sr_4Co_3O_{7.5}Cl_2$ and 3.86585(3) Å for $Sr_4Mn_3O_{7.56}Cl_2$). The $M1O_6$ octahedra in $Ca_4Fe_{3-x}Mn_xO_{8-\delta}Cl_2$ is similar to that in $Ca_4Mn_3O_{10}$ [26], with both tilting (~9°) and rotation (~10.5°), clearly manifested by the structural splitting of O1 and O2 (Fig. 2b). This is attributed to the small *a* parameters (Table 1) relative to those of the related Sr-compounds mentioned above. Nevertheless, from the single-crystal X-ray diffraction data, it is not possible to determine unambiguously if oxygen deficiency exists at the O1 site in $Ca_4Fe_{3-x}Mn_xO_{8-\delta}Cl_2$. A relatively large amount of polycrystalline sample of $Ca_4Fe_{3-x}Mn_xO_{8-\delta}Cl_2$ with homogeneous stoichiometry could not be obtained by typical solid state reactions, for a possible PND study.

As shown in Fig. 3, the ^{57}Fe Mössbauer spectra of two samples of $Ca_4Fe_{3-x}Mn_xO_{8-\delta}Cl_2$, $x=0.92$, and 1.36 are almost identical, and both indicate three distinct Fe cations with very similar distributions, which confirm the structural disordering of Mn/Fe. The isomer shifts (IS) and quadrupole splittings (QS), for two of the unique Fe ions with ~57% and ~35%, respectively, are typical for Fe^{3+}; however, the valence state of the third Fe (~8%) is not certain from the IS and QS data.

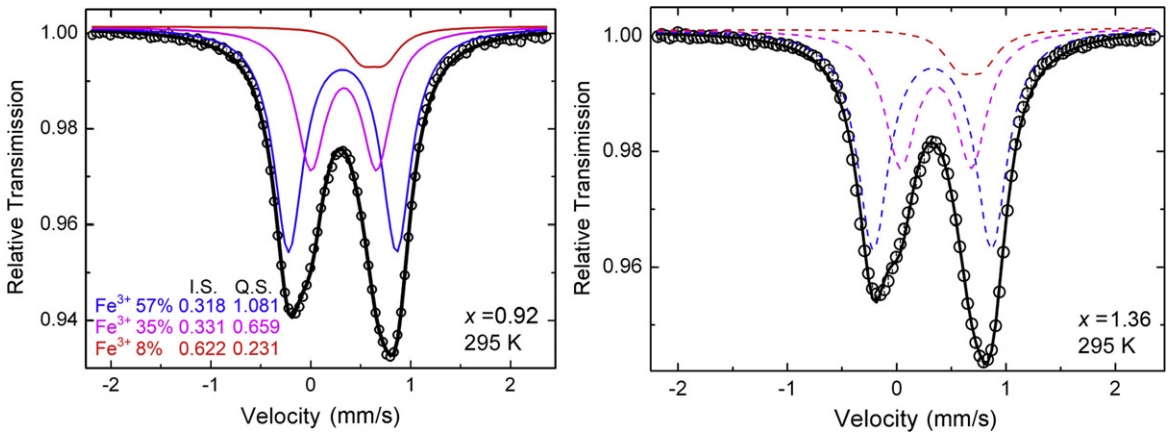

Fig. 3. ^{57}Fe Mössbauer Spectra of $x=0.92$ and 1.36 samples.

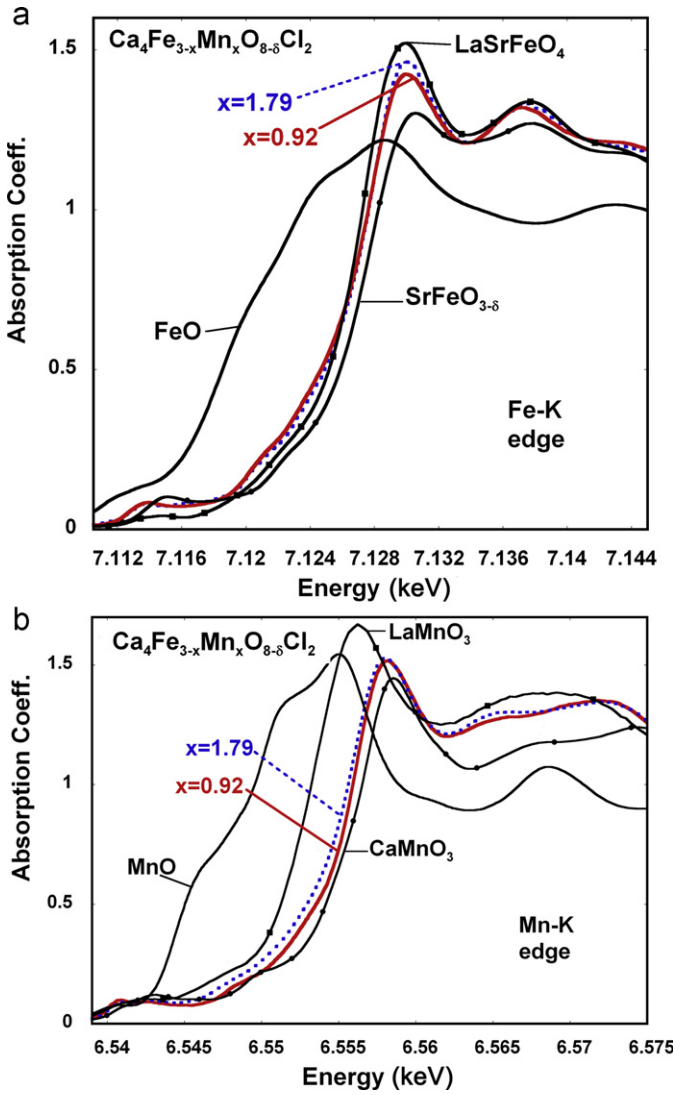

Fig. 4. Fe- and Mn–K edge XAS spectra for $x=0.92$ and 1.79 samples along with the standards.

The XAS results of two members of $Ca_4Fe_{3-x}Mn_xO_{8-\delta}Cl_2$ ($x=0.92$, 1.79) in Fig. 4a show that all the Fe ions are trivalent. Moreover, the large Mn^{4+} content in $Ca_4Fe_{3-x}Mn_xO_{8-\delta}Cl_2$ (Fig. 4b) would likely oxidize any Fe^{2+} to Fe^{3+} (assuming redox potentials similar to those in aqueous solution) [27], and Fe^{4+} is unlikely to coexist with $Mn^{3+/4+}$. Therefore, we assign the unique ~8% Fe seen in the Mössbauer to be also Fe^{3+}. In this scenario, the presence of oxygen deficiency is the only possible explanation for the observation of the ~8% Fe in the Mössbauer. As already discussed above, the oxygen deficiency can only be at the O1 site. Thus the three unique Fe^{3+} are assigned to: $Fe2O_5Cl$ (57%), $Fe1O_6$ (~35%) and $Fe1O_5$ (~8%); In Fig. 4b the Mn–K edges of two members of $Ca_4Fe_{3-x}Mn_xO_{8-\delta}Cl_2$ along with Mn^{2+}, Mn^{3+} and Mn^{4+} standards indicate fairly conclusively that the formal oxidation state of Mn is close to 4+ in the $x=0.92$ and 1.79 phases.

The ratio of $Fe1O_5$ to $Fe1O_6$ provides some insight on the level of oxygen deficiency (δ). It is clear that the upper limit of the O1 vacancy is 1/4, equal to 100% $M1O_5$ to 0% $M1O_6$. If the O1 vacancy is 1/4, then, $\delta=0.5$, which is exactly the case in $Sr_4Co_3O_{7.5}Cl_2$ [15]. For example, in $Ca_4Fe_{2.08}Mn_{0.92}O_{8-\delta}Cl_2$ the Fe ratios obtained from ^{57}Fe Mössbauer spectra gives at M1: $0.73Fe1O_6+0.17Fe1O_5+0.10Mn1O_n$ together with $1.18Fe2O_5Cl+0.82Mn2O_5Cl$ at the M2 position. Since we do not know the ratio of $Mn1O_5$ to $Mn1O_6$, δ can only be roughly estimated to be between 0.085 (the case of 100% $Mn1O_6$) to 0.135 (the case of 100% $Mn1O_5$). Therefore, the formal valence state of Mn is between 3.8+ ($\delta\sim0.135$) and 3.90+ ($\delta\sim0.085$), is consistent with the XAS results (Fig. 4b). In any case, Mn^{4+} is much more dominant than Mn^{3+}. With higher x values, more Fe^{3+} are replaced by Mn cations, and the XAS indicates a discernable but modest decrease of the Mn valence to ~3.6 in the $x=1.79$ phase. The oxygen deficiency in $Ca_4Fe_{1.21}Mn_{1.79}O_{8-\delta}Cl_2$ cannot be very high, because the XAS result indicates that the formal valence state of Mn is much closer to 4+ than 3+. We conclude that, in the solid state solution of $Ca_4Fe_{3-x}Mn_xO_{8-\delta}Cl$, the Mn valence state changes from mostly Mn^{4+} ($x=0.92$) to more mixed-valent at $x=1.79$.

In Fig. 5a the ZFC-FC temperature-dependent magnetic susceptibility data ($\chi=M/H$) of six samples of $Ca_4Fe_{3-x}Mn_xO_{8-\delta}Cl_2$ ($0.92\leq x\leq1.79$) indicate very small susceptibility values, which suggest strong and predominantly antiferromagnetic (AFM) interactions. Fitting the data to *Curie–Weiss* law of all the samples resulted in unreasonable parameters (Table 4) similar to that shown in Fig. 5b for $Ca_4Fe_{1.21}Mn_{1.79}O_{8-\delta}Cl_2$ (i.e. $\mu_{eff}=6.56\mu_B$, much lower than the expected spin-only value ($\sim14\mu_B$). Such large deviations from *Curie–Weiss* behavior indicate that the samples already at ~300 K have short-range AFM ordering. At low temperature, clear spin-glass behavior of all samples is observed, as expected due to the high level of disordering of Mn and Fe. The isothermal magnetizations for $x=1.19$ and 1.53 samples at 5 K (Fig. 5c) show slow linear increases below 3 T with small loops, which are consistent with strong AFM interactions and spin-glass behavior.

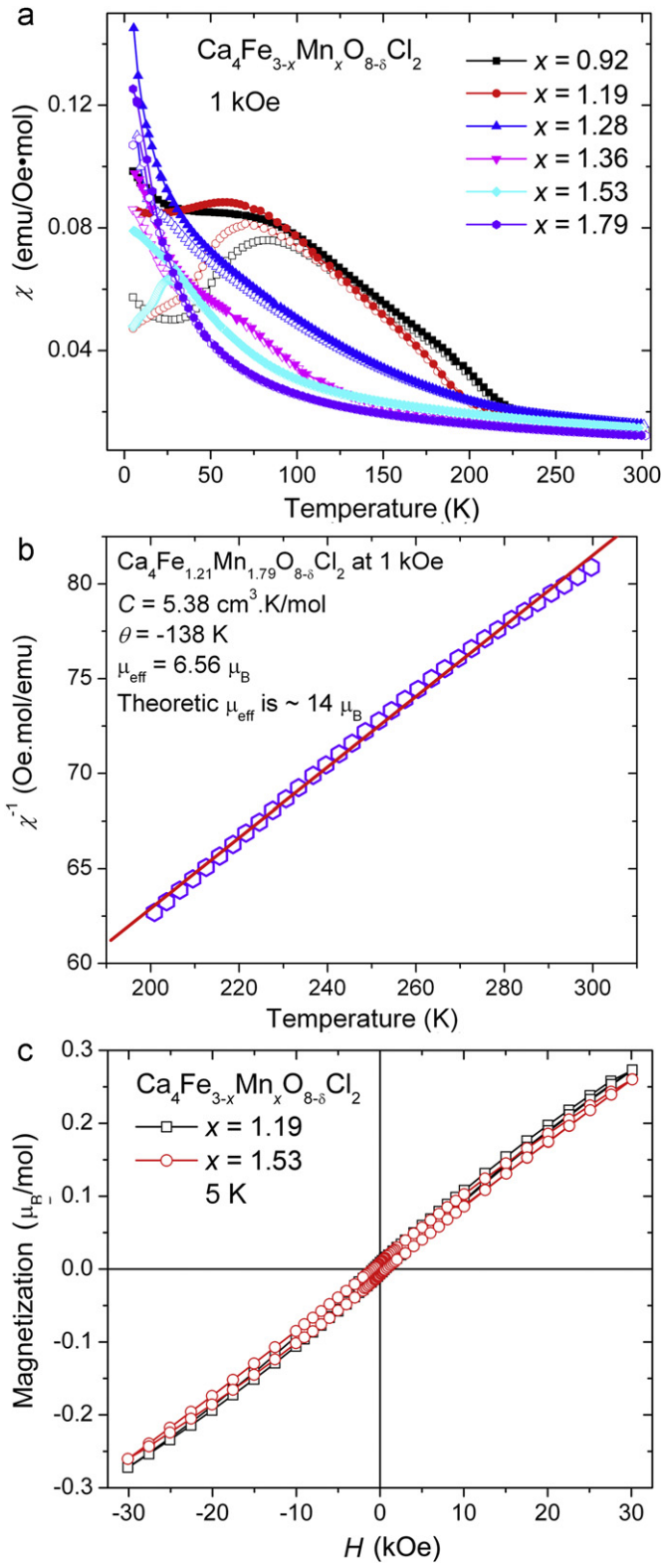

Fig. 5. (a) Temperature-dependent magnetic susceptibilities for the samples with $0.92 \leq x \leq 1.79$; (b) *Curie–Weiss* fitting using the data above 200 K for $x=1.79$ and (c) isothermal magnetizations at 5 K for samples with $x=1.19$ and 1.53.

4. Conclusion

Solid solutions of $Ca_4Fe_{3-x}Mn_xO_{8-\delta}Cl_2$ ($0.92 \leq x \leq 1.79$) single crystals were prepared in $CaCl_2$ flux in an open system, resulted in the third examples of $n=3$ Ruddlesden–Popper oxychlorides. All samples crystalize in space group *I*4/*mmm*. Due to the tilting and rotation of the $(Mn/Fe)O_6$ octahedra, the O1 and O2 sites are split into partially occupied special positions and refine in a ring-like distribution. A low level of oxygen deficiency at O1 is deduced ($\delta \sim 0.1$), leading to MnO_5/FeO_5 square-pyramids. The ^{57}Fe Mössbauer and XAS studies indicate that all the Fe ions are trivalent, while the formal oxidation state of Mn varies from very close to 4+ in the $x=0.92$ member ($\sim$3.8–3.9) to mixed-valent $Mn^{3+/4+}$ in the $x=1.79$ member ($\sim$3.6). Magnetic investigations indicate short-range antiferromagnetic ordering already at room temperature and spin-glass behavior at low temperature due to the structural disordering of Mn/Fe.

Table 4
Curie–Weiss parameters for the samples $Ca_4Fe_{3-x}Mn_xO_{8-\delta}Cl_2$ ($0.92 \leqslant x \leqslant 1.79$). Theoretical μ_{eff} was roughly estimated, assuming 3.9μ_B for Mn^{4+}, 4.9μ_B for Mn^{3+}, and 5.9μ_B for Fe^{3+}.

x	Temperature range (K)	C (cm^3 K/mol)	θ (K)	Exp μ_{eff} (μ_B)	Theo μ_{eff} (μ_B)
0.92	250–300	4.45	−14	5.96	16
1.19	250–300	4.98	−39	6.31	15
1.28	250–300	5.66	−55	6.73	15
1.36	200–300	4.88	−80	6.25	15
1.53	200–300	6.37	−134	7.14	14
1.79	200–300	5.38	−138	6.56	14

Acknowledgment

This work was partially supported by NSF-DMR 0541911 grant (MG, TY).

Appendix A. Supplementary material

Supplementary data associated with this article can be found in the online version at doi:10.1016/j.jssc.2010.03.019.

References

[1] S. Jin, T.H. Tiefel, M. McCormack, R.A. Fastnacht, R. Ramesh, L.H. Chen, Science 264 (1994) 413–415.
[2] Y. Moritomo, A. Asamitsu, H. Kuwahara, Y. Tokura, Nature (London) 380 (1996) 141–144.
[3] S.N. Ruddlesden, P. Popper, Acta Crystallogr. 10 (1957) 538–539.
[4] C. Brisi, M. Lucco-Borlera, Atti Acad. Sci. Torino 96 (1961–1962) 805–810.
[5] C. Brisi, Ann. Chim. (Rome) 51 (1961) 1399–1403.
[6] C. Brisi, M. Lucco-Borlera, J. Inorg. Nucl. Chem. 27 (1965) 2129–2132.
[7] J.C. Bouloux, J.L. Soubeyroux, G. Le Flem, P. Hagenguller, J. Solid State Chem. 38 (1981) 34–39.
[8] J.F. Mitchell, J.E. Millburn, M. Medarde, S. Short, J.D. Jorgensen, J. Solid State Chem. 141 (1998) 599–603.
[9] N.S. Witte, P. Goodman, F.J. Lincoln, R.H. March, S.J. Kennedy, Appl. Phys. Lett. 72 (1998) 853–855.
[10] M.D. Carvalho, R.P. Borges, A.V. Girão, M.M. Cruz, M.E. Melo Jorge, G. Bonfait, P. Dluzewski, M. Godinho, Chem. Mater. 17 (2005) 4852–4857.
[11] P. Chai, X.J. Liu, M.F. Lu, Z.L. Wang, J. Meng, Chem. Mater. 20 (2008) 1988–1996.
[12] W.J. Lu, Y.P. Sun, R. Ang, X.B. Zhu, W.H. Song, Phys. Rev. B 75 (2007) 014414.
[13] C.S. Knee, M.T. Weller, Chem. Commun. (2002) 256–257.
[14] C.S. Knee, A.A. Zhukov, M.T. Weller, Chem. Mater. 14 (2002) 4249–4255.
[15] S.M. Loureiro, C. Felser, Q. Hunag, R.J. Cava, Chem. Mater. 12 (2000) 3181–3185.
[16] B. Grande, H. Müller-Buschbaum, Z. Anorg. Allg. Chem. 417 (1975) 68–74.
[17] B. Grande, H. Müller-Buschbaum, Z. Anorg. Allg. Chem. 429 (1977) 88–90.
[18] T. Sowa, M. Hiratani, K. Miyauchi, J. Solid State Chem. 84 (1990) 178–181.
[19] J. Huang, R.D. Hoffmann, A.W. Sleight, Mater. Res. Bull. 25 (1990) 1085–1090.
[20] C.S. Knee, M.T. Weller, J. Solid State Chem. 168 (2002) 1–4.
[21] W. Leib, H. Müeller-Buschbaum, Z. Anorg. Allg. Chem. 518 (1984) 115–119.

[22] C.S. Knee, M.A.L. Field, M.T. Weller, Solid State Sci. 6 (2004) 443–450.
[23] J.F. Ackerman, J. Solid State Chem. 92 (1991) 496–513.
[24] TOPAS V2.1: General Profile and Structure Analysis Software for Powder Diffraction Data; Bruker AXS, Karlsruhe, Germany.
[25] G.M. Sheldrick, SHELXS 97, Program for the solution of crystal structures, University of Göttingen, Göttingen, Germany, 1997. SHELXL 97, Program for the refinement of crystal structures, University of Göttingen, Göttingen, Germany, 1997.
[26] P.D. Battle, M.A. Green, J. Lago, J.E. Millburn, M.J. Rosseinsky, J.F. Vente, Chem. Mater. 10 (1998) 658–664.
[27] Langes Chemistry Handbook 15th Sec. 8. Electrolytes, Ctromotive Force, and Chemical Equilibrium, 1998.